Geophys. J. Int. (2007) **171,** 909–920 doi: 10.1111/j.1365-246X.2007.03550.x

Comparison of seismic moment release rates along different types of plate boundaries

Cliff Frohlich[1] and Laura Reiser Wetzel[2]

[1]*Institute for Geophysics, Jackson School of Geosciences, University of Texas at Austin,* 10100 *Burnet Road* (R2200) *Austin, TX* 78758-4445*, USA. E-mail: cliff@ig.utexas.edu*

[2]*Department of Marine Science, Eckerd College,* 4200 54th *Ave. S., St. Petersburg, FL* 33711*, USA*

Accepted 2007 July 19. Received 2007 July 16; in original form 2007 March 9

SUMMARY

This is a global survey of seismic moment release rates (scalar moment/length/time) along five categories of plate boundaries; for shallow earthquakes we evaluate divergent, transcurrent and convergent boundaries; for deep earthquakes we consider separately boundaries where the deepest seismicity is intermediate (<300 km) or deep-focus (500–600 km). The objective is to evaluate the typical range of rates observed and present the results in a form where it is straightforward to compare factors that affect rates in the different environments. For earthquakes occurring 1977–2005, the data are scalar moments from the global centroid moment tensor catalogue; for earthquakes 1900–1976, we use a standard formula to obtain moment from magnitudes in the Engdahl–Villaseñor Centennial catalogue. Moment release rates correlate with relative velocity between plates along divergent and transcurrent boundaries; focal depth influences moment release rates along intermediate and deep-focus boundaries. After accounting for these effects and adjusting rates for the influence of the short (29–106 yr) data record, within each category the typical observed variation is about an order of magnitude. We estimate seismic coupling coefficients, that is, the proportions of plate tectonic slip accommodated as earthquake rupture and reflected in the moment rates. Coupling may be 0.7 or greater along shallow convergent boundaries where at least one plate is continental. For all other boundary categories coupling is generally less than 0.4; it is 0.2 or less along most divergent boundaries and for intermediate and deep boundaries at depths exceeding 100 km. These results confirm that there are fundamental mechanical differences in the failure processes acting along different categories of plate boundaries. One implication is that only along a few highly coupled boundaries is it plausible that analysis of seismicity alone might lead to successful algorithms to predict large earthquakes.

Key words: deep earthquakes, earthquake mechanism,earthquake prediction, plate tectonics,seismic moment.

1 INTRODUCTION

The success of plate tectonic theory rests on the observation that geological features differ markedly along divergent, transcurrent and convergent plate boundaries, and these differences are attributable to the distinctly different mechanical environments at shallow depths along each type of boundary as well as at greater depths where intermediate and deep-focus earthquakes occur. Seismic activity reflects these differences, as the largest observed earthquakes and predominant focal mechanisms also differ among the various types of boundaries. However, for each type, how important is the seismicity mechanically, that is, what fraction of the moment release do earthquakes accommodate? Determining the so-called 'seismic coupling coefficients' at various shallow plate boundaries has been the subject of numerous papers (e.g. Bird *et al.* 2002; Bird & Kagan 2004), including some that focus on only one category of boundary (e.g. subduction zones: Peterson & Seno 1984; Jarrard 1986; Pacheco *et al.* 1993; oceanic transforms: Boettcher & Jordan 2004).

Measuring seismic coupling is problematic because rare very large earthquakes often produce the majority of the moment release and thus uncertainties are huge (e.g. McCaffrey 1997b), especially since some very large earthquakes may rupture the lithosphere to greater depths than smaller, 'ordinary' earthquakes. Moreover, while the length along a plate boundary is relatively easy to measure, the thickness of the seismogenic zone is uncertain, and an easier-to-determine quantity is the product of thickness and the coupling coefficient, which Bird & Kagan (2004) call the 'coupled seismic thickness'.

Like Bird & Kagan (2004), the present study will compare measures of moment release rates for different tectonic categories

© 2007 The Authors
Journal compilation © 2007 RAS

Table 1. Summary of variables used in this paper.

Variable	Explanation	Equation or figure
M_o	Seismic moment, equal to the product of rigidity μ, fault area LW, and slip S	Eq. (2)
β	Exponent of moment distribution	Eq. (3)
T, $T_{standard}$	Time interval covered by earthquake catalogue; standard interval for adjustments	Eqs (2)–(6)
R_{annual}, $R_{annual-GR}$, $R_{adjusted-1}$, $R_{adjusted-2}$	Annual moment release rates, simple and adjusted	Eqs (2), (4)–(6)
R_{thrust}, $R_{strike-slip}$, R_{normal}, R_{int}, R_{deep}	Annual moment release rates in different tectonic environments	Eq. (8)
M_T, M_C	'threshold' magnitude of completeness for catalogue; cut-off or maximum magnitude where β no longer applies	Eqs (3), (4), (6) and (7)
N_{large}	Estimate of number of earthquakes necessary before moment rates need no adjustment	Eq. (7)
$L_{\|\|}$, $L_\perp$	Length of plate boundary along or perpendicular to velocity vector V	Eq. (8)
r_{conv}, r_{trans}, r_{div}, r_{int}, r_{deep}	Moment release rates normalized for boundary length and velocity	Eq. (8), Figs 3–8
W_{conv}, W_{trans}, W_{div}, W_{int}, W_{deep}	Coupled thicknesses or effective seismic widths (equals fault width if no aseismic slip occurs along plate boundary)	Eq. (9), Figs 3–6
$W_{estimate}$	Estimated fault width	Eq. (10)
C_{conv}, C_{trans}, C_{div}, C_{int}, C_{deep}	Coupling coefficients (fraction of motion that occurs seismically)	Eqs (10) and (11), Figs 3–8
$S_{seismic}$, S_{PT}	Seismic slip and total slip along plate boundary	Eqs (10) and (11)

of plate boundaries. However, our study differs in several ways. First, we apply a different, recently developed statistical procedure (Frohlich 2007) to address the large-earthquake problem. Our approach is less rigorous but computationally much simpler than that of Bird and Kagan; for example, we assess uncertainty by calculating moment rates by several different methods. However, generally the two methods obtain very similar quantitative results. Second, unlike any previous study, we evaluate moment release and measures of coupling for intermediate- and deep-focus earthquakes as well as for shallow seismicity. And finally, whereas Bird and Kagan divided shallow earthquakes into seven tectonic categories and determined coupled seismic thicknesses and coupling coefficients for each, we instead consider only three categories (divergent, transform and convergent) and focus on evaluating how their properties depend on relative plate velocity.

The principal products of our analysis are graphs of moment rate versus relative plate velocity and focal depth that allow for a straightforward comparison of seismic moment release between fundamentally different tectonic environments. To avoid confusion about notation, Table 1 presents a summary of the variables used in this paper and indicates where they are summarized in figures.

2 DATA AND METHODS

2.1 Earthquake data and plate boundary selection

For primary data we use moments and magnitudes as reported in two catalogues (Fig. 1): the Engdahl & Villaseñor (2002) centennial (EVC) catalogue and the global centroid moment tensor (GCMT) catalogue. The GCMT catalogue was formerly known as the Harvard CMT catalogue (e.g. Dziewonski & Woodhouse 1983; Ekström *et al.* 2005), but has been renamed since the routine processing of CMT is now managed at Columbia University. Together these catalogues cover 106 yr from 1900 to 2005; the GCMT catalogue is complete down to a magnitude approaching 5.5. The EVC catalogue doesn't report moment magnitudes M_W for all earthquakes; however for events before 1976 it reports a preferred magnitude determined by incorporating information from various other sources (e.g. Abe 1981, 1984; Pacheco & Sykes 1992; Huang *et al.* 1997, 1998; Chen *et al.* 2001). When several magnitude determinations are available, for shallow earthquakes ($h < 60$ km) their order of preference is M_W, M_S, m_B and m_b; for deep earthquakes ($h \geq 60$ km) it is M_W, m_B and m_b. Engdahl & Villaseñor (2002) indicate their catalogue

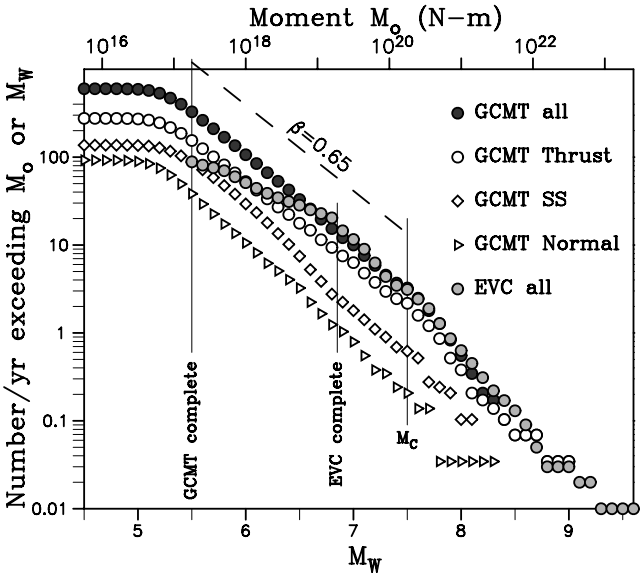


Figure 1. Cumulative annual number of shallow earthquakes ($h < 60$ km) with moments exceeding M_o or magnitudes exceeding M_W as reported in the GCMT (black circles) and Engdahl & Villaseñor (2002) Centennial (EVC) (grey circles) catalogues. The catalogues are nearly complete for moment magnitudes M_W exceeding about 5.5 and 6.85, respectively. For the GCMT catalogue the plot indicates rates for all events (black circles) as well as thrust (white circles), strike-slip (diamonds) and normal-faulting (triangles) mechanisms. Note the relative proportions of events with different mechanisms and also that there is an apparent change in the slope or β-value for all earthquakes and for GCMT thrusts at about M_W of 7.5.

is effectively complete for magnitudes M_S of 7.0 and greater since 1900; for 6.5 and greater since 1930; and 5.5 and greater since 1964.

We used the standard relationship to convert M_W to M_o:

$$\log M_o[\mathrm{N-m}] = 1.5M_W + 9. \quad (1)$$

When the preferred magnitudes were M_S, m_B and m_b we adjusted them to M_W using the curves in Utsu's (2002) so-called master graph; for earthquakes prior to 1960 with preferred magnitudes originally from Gutenberg & Richter (1954), Båth & Duda (1979) and Rothé (1969), we followed Engdahl & Villaseñor (2002) and reduced the magnitudes by 0.2 before performing the M_S to M_W conversion.

© 2007 The Authors, *GJI*, **171,** 909–920
Journal compilation © 2007 RAS

For plate boundaries we used an updated version of those described by Coffin *et al.* (1998). For each plate boundary segment of length L_k, we calculated the angle α between the strike of the segment and the relative motion vector from DeMets *et al.* (1994), and thus determined the effective total lengths $L_{||} = \Sigma L_k \sin\alpha$ and $L_\perp = \Sigma L_k \cos\alpha$ parallel and perpendicular to the boundary. Generally, we associated earthquakes with a boundary if their reported locations lay within 100 km of the boundary.

We categorized earthquakes in the GCMT catalogue as normal, strike-slip, or thrust depending on whether the *P*-, *B*- or *T*-axis was most nearly vertical (Frohlich & Davis 1999; Frohlich 2001). Focal mechanism information is not generally available for EVC earthquakes occurring prior to 1976. However, along convergent margins thrusts dominate moment release and along oceanic ridge-transforms strike-slip earthquakes are dominant. Thus in these environments we compare moment sums for the EVC and GCMT catalogues.

2.2 Moment release rates

If we observe that N earthquakes occur over time T years along a plate boundary of length L, the simplest measure of moment release rate R_{annual} is:

Simple rate:

$$R_{\text{annual}} = \sum_{i=1}^{N} \frac{M_{o-i}}{T}. \tag{2}$$

If moments are distributed according to the so-called Gutenberg & Richter (1956) or Ishimoto and Iida (1939) distribution, where M_T is a threshold moment for which the observations exceeding M_T are uniform and complete, the cumulative fraction F_{GR} with moments exceeding M_o is:

Gutenberg–Richter (GR):

$$F_{GR} = \left(\frac{M_T}{M_o}\right)^{\beta}. \tag{3}$$

As discussed by Frohlich (2007), the simple rate R_{annual} suffers from two problems. First, as T or N increase the expected value for R_{annual} increases indefinitely, never converging at a finite value; for example, if $N_{T=1\,\text{yr}}$ is the annual number of earthquakes exceeding a completeness threshold moment M_T, then the expected value for (1) is:

$$R_{\text{annual-GR}} = \frac{\beta}{1-\beta} M_T N_{T=1\text{yr}}^{1/\beta} T^{\frac{1}{\beta}-1}. \tag{4}$$

Thus to compare rates for GR-distributed events it is important to adjust the observed rates to correspond to a standard time period T_{standard}, that is:

Time-adjusted rate:

$$R_{\text{adjusted}-1} = R_{\text{annual}} \left(\frac{T_{\text{standard}}}{T}\right)^{\frac{1}{\beta}-1}. \tag{5}$$

For GR-distributed moments a second problem is that the simple rate R_{annual} depends strongly on the largest event observed; indeed, for representative values of β near 0.60 the largest earthquake typically is responsible for half of more of R_{annual}. One way to avoid this is to time-adjust eq. (4) and determine the rate from the number of events exceeding any convenient threshold magnitude, that is:

Size-adjusted rate:

$$R_{\text{adjusted}-2} = \frac{\beta}{1-\beta} M_T N_{T=1\text{yr}}^{1/\beta} T_{\text{standard}}^{\frac{1}{\beta}-1}. \tag{6}$$

It's worth noting that this is only an improvement if one has confidence in the value chosen for β.

Of course, in practice moments cannot satisfy a GR distribution for very large earthquakes, since above some cut-off moment M_C they must fail to occur or occur at greatly reduced rates (e.g. Kagan 1997). Frohlich (2007) shows that for earthquakes distributed according to a truncated GR or exponentially tapered GR (Kagan) distribution, a useful number for assessing this is:

$$N_{\text{large}} = \left(\frac{M_C}{M_T}\right)^{\beta}. \tag{7}$$

When the number of observations $N > N_{\text{large}}$ the rate R_{annual} from eq. (2) is representative of the long-term moment release rate; alternatively, when $N < N_{\text{large}}$ the rate changes over time as in eq. (4) and thus it is reasonable to adjust it for a particular time period as in eqs (5) and (6). Note that N_{large} is just $1/F_{GR}$ when M_o equals M_C (eq. 3) and is approximately equivalent to the number of events that must be sampled before one is likely to find one GR event with moment exceeding M_C. Thus for smaller N the distribution is GR-like and the rate R_T (eq. 2) increases with time; for larger N, rates are stable as for the truncated or tapered distribution.

2.3 What the present study reports

To assess moment rates along shallow plate boundaries (see Fig. 2) this paper will use eqs (2), (5) or (6) to calculate the moment rates R_{thrust}, $R_{\text{strike-slip}}$ and R_{normal} for earthquakes with thrust, strike-slip and normal mechanisms, adjusting the rates to a standard period T_{standard} of 100 yr when $N < N_{\text{large}}$. To facilitate comparisons we divide moment rates by $L_{||}V$ or $L_\perp V$, where V is the mean relative motion of the plates as determined from DeMets *et al.* (1994) and $L_{||}$ and $L_\perp$ are the parallel and perpendicular components of the plate boundary length. Thus, the left vertical axes for figures displaying results for convergent, transform and divergent boundaries show:

Moment rates:

$$r_{\text{conv}} = \frac{R_{\text{thrust}}}{L_\perp V} \quad r_{\text{trans}} = \frac{R_{\text{strike-slip}}}{L_{||} V} \quad r_{\text{div}} = \frac{R_{\text{normal}}}{L_\perp V}. \tag{8}$$

For convenience the right vertical axes display the same results in units that are more intuitive. Moment is μLWS_{seismic}, where μ is rigidity, L is along-strike fault length, W is downdip fault width and S_{seismic} is the average slip radiated seismically by the fault; thus over sufficient time T plate motion will occur along the entire length L of a plate boundary and produce plate tectonic slip $S_{PT} = VT$. Thus if we divide the quantities r_{conv}, r_{trans} and r_{div} in eq. (8) by μ we obtain coupled thickness W_{conv}, W_{trans} and W_{div} for convergent, transform or divergent faults along the boundary; for example:

Coupled-seismic thickness:

$$W_{\text{conv}} = \frac{r_{\text{conv}}}{\mu}. \tag{9}$$

These 'coupled thicknesses' or 'effective seismic widths' (Brune 1968) equal the fault width W if during time T the plates move freely and there is no aseismic slip; that is, all the plate motion is expressed as radiated seismic moment. Thus if we arbitrarily choose a fault width W_{estimate} and further divide, we obtain estimates of the coupling coefficients C_{conv}, C_{trans} and C_{div} of plate motion (Scholz 2002); for example:

Coupling coefficients:

$$C_{\text{conv}} = \frac{W_{\text{conv}}}{W_{\text{estimate}}} \approx \frac{S_{\text{seismic}}}{S_{PT}}. \tag{10}$$

© 2007 The Authors, *GJI*, **171,** 909–920
Journal compilation © 2007 RAS

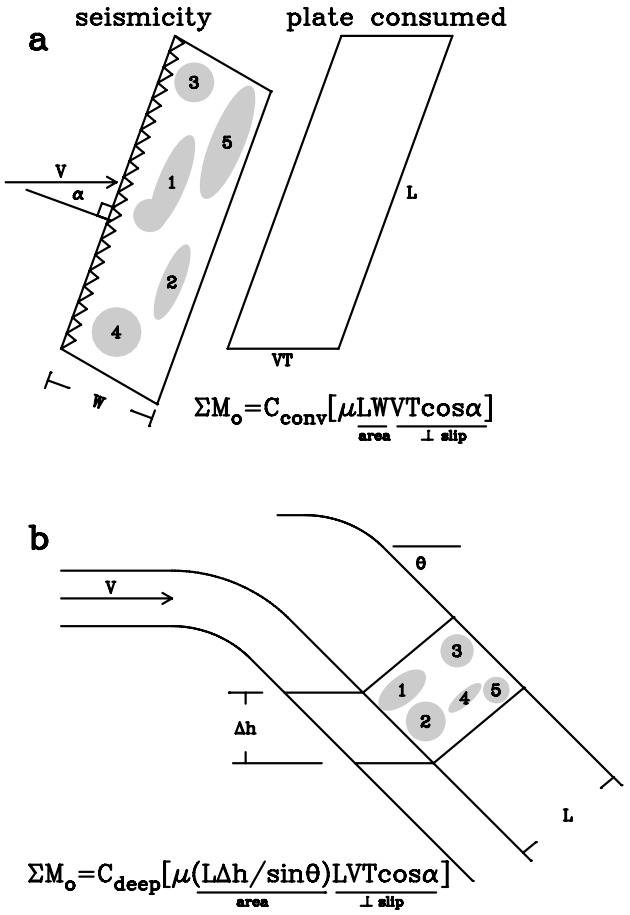


Figure 2. Relationship between seismic moment release and relative plate motion (a) along a convergent plate boundary; and (b) within a Wadati–Benioff zone. During time period T there is perpendicular convergence $VT\cos\alpha$ producing slip along a fault with area LW; if all of this slip is associated with earthquake ruptures (numbered shaded areas) the coupling coefficient $C_{\rm conv}$ is 1.0. Along the shallow plate boundary (a) we have little direct information about the width W of the seismically active zone; within Wadati–Benioff zones (b) there is seismic activity over a range of depths and thus we can divide the subducting lithosphere into zones of width $\Delta h/\sin\theta$.

Calculating values for adjusted moment rates (eqs 5, 6 and 8) requires choosing appropriate values for β. There are a wide range of values of β reported in the literature depending on the catalogue chosen, the events selected and the method used to determine β (e.g. see Frohlich & Davis 1993; Kagan 1999; Bird *et al.* 2002; Bird & Kagan 2004). For shallow thrust earthquakes along convergent margins we follow Kagan (1999) and use β of 0.60. For oceanic divergent and transform boundaries Bird *et al.* (2002) found β to be 2/3; however, we choose β of 0.75 because this is in closer agreement with the data plotted in Fig. 1 for magnitudes between $M_{\rm W}$ of 5.5–7.5. For intermediate and deep events we did not adjust moment rates and thus no assumption about β was necessary (see eq. 2).

Calculating values for the coupled seismic thickness (eq. 9), and coupling coefficients (eq. 10) requires values for the rigidity μ and fault widths $W_{\rm estimate}$. For μ at crustal depths, Stacey (1992) reports values of 26.6–44.1 GPa; Bird & Kagan (2004) assume μ of $\sim$25 $\pm$ 5 GPa for oceanic ridge-transforms and $\sim$50 $\pm$ 20 GPa for subduction zones. In this paper, we will assume that $\mu = 50$ GPa for subduction zones and 30 GPa for ridge-transforms. Estimates of $W_{\rm estimate}$ are highly variable, even for earthquakes in similar tectonic environments (see discussion in Kagan 1999 and McCaffrey 1997a). However, for most subduction zones Tichelaar & Ruff (1993) find a maximum depth of faulting of about 40 km; thrust faults are non-vertical so in this paper for $W_{\rm estimate}$ we use 60 km for thrust and 40 km for strike-slip earthquakes. On spreading ridges centroid depths for earthquakes are typically 3–5 km (Solomon *et al.* 1988; Rundquist & Sobolev 2002); the normal faults generating them should extend deeper and have plunges of $\sim$45°; in this paper we use 10 km for $W_{\rm estimate}$. For transform faults we arbitrarily choose an intermediate value of 20 km for $W_{\rm estimate}$.

For intermediate- and deep-focus earthquake zones we use the compilation of Frohlich (2006) to evaluate the along-strike length L of the Wadati–Benioff zone at depth increments Δh of 20 km. Then, we calculate the moment sums $R_{\rm int}$ and $R_{\rm deep}$ using eq. (2) and determine $r_{\rm int} = \frac{R_{\rm int}}{LV_\perp}$ and $r_{\rm deep} = \frac{R_{\rm deep}}{LV_\perp}$.

Hence:

$$C_{\rm int} = \frac{r_{\rm int}}{\mu \Delta h \sin\theta} \approx \frac{S_{\rm seismic}}{S_{\rm PT}};\ C_{\rm deep} = \frac{r_{\rm deep}}{\mu \Delta h \sin\theta} \approx \frac{S_{\rm seismic}}{S_{\rm PT}}. \quad (11)$$

Here $V_\perp$ is the component of plate motion perpendicular to the plate boundary and θ is the dip of the Wadati–Benioff zone. Of course, θ and μ may change with depth and/or differ in different zones. Thus for simplicity in plots of moment rate we fix θ to be 45° and use 70 GPa for μ which corresponds approximately to 200 km depth (Stacey 1992).

3 RESULTS

3.1 Divergent plate boundaries

Along 16 divergent boundaries the moment rates generally decrease about a factor of 10 as the plate divergence velocity increases from less than 1 cm yr^{-1} to about 7.5 cm yr^{-1} (Fig. 3 and Tables 2

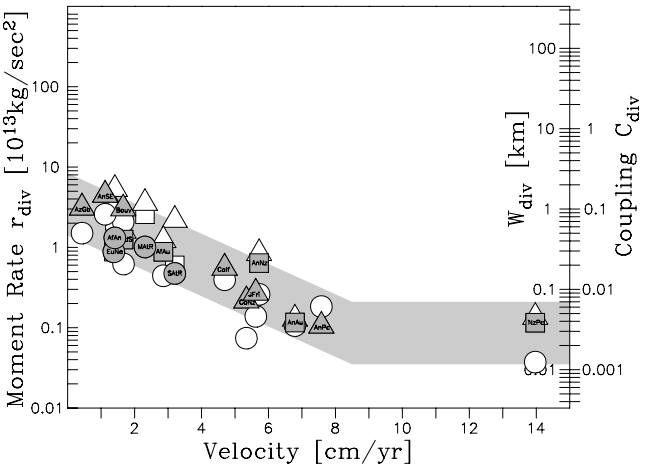


Figure 3. Divergent plate boundaries: Dependence on relative plate velocity of moment rate $r_{\rm div}$ (eq. 8), coupled thickness $W_{\rm div}$ (see eq. 9) and coupling coefficient $C_{\rm div}$ (see eq. 10) for normal-faulting GCMT earthquakes occurring 1977–2005 along divergent plate boundaries. Circles correspond to values determined directly from simple rate (eq. 2). Squares and triangles correspond to values adjusted to $T_{\rm standard}$ of 100 yr (see eq. 6) and determined from the 10th largest earthquake (squares) or number of events exceeding the threshold magnitude of 5.5 (triangles). Filled symbol designates value preferred after considering $N_{\rm large}$ (eq. 7) and number of events on each boundary; all calculations assume $\beta = 0.75$, $\mu = 30$ GPa, and a cut-off moment $M_{\rm C}$ corresponding to magnitude $M_{\rm W}$ of 6.75 as indicated in Table 3; calculation of $W_{\rm div}$ assumes $W_{\rm estimate} = 10$ km. Shaded region indicates approximate trend of the data.

© 2007 The Authors, *GJI*, **171,** 909–920
Journal compilation © 2007 RAS

Table 2. Plate boundaries evaluated in this study. Abbreviation column indicates abbreviations used in Figs 3–8 and Tables 3–8. Plates key: Af – Africa; An – Antarctica; Ar – Arabia; Au – Australia; Ca – Caribbean; Co – Cocos; Jf – Juan de Fuca; Eu – Eurasia; In – India; Na – North America; Nz – Nazca; Pc – Pacific; Ph – Philippines; Sa – South America and Sc – Scotia. In this table the entries 'CMT' refer to the GCMT catalogue.

Geographic name	Abbre-viation	Plates	Divergent – Fig. 3 and Table 3	Transform – Fig. 4 and Table 4	Convergent-thrust– Fig. 5 and Table 5	Convergent-stike-slip – Fig. 6 and Table 6	Intermediate– Fig. 7 and Table 7	Deep – Fig. 8 and Table 8
Africa–Antarctica	AfAn	Af-An	CMT	CMT, EVC				
Red Sea	RedS	Af-Ar	CMT	CMT				
Africa–Australia	AfAu	Af-Au	CMT	CMT, EVC				
Italy–Greece	ItGr	Af-Eu			CMT, EVC	CMT		CMT, EVC
Greece–Turkey	GrTu	Af-Eu					CMT, EVC	
Azores–Gibralter	AzGb	Af-Eu	CMT	CMT, EVC				
Mid-Atlantic Ridge	MAtR	Af-Na	CMT	CMT				
South-Atlantic Ridge	SAtR	Af-Sa	CMT	CMT, EVC				
Antarctic–Australia	AnAu	An-Au	CMT	CMT				
Antarctic-Nazca	AnNz	An-Nz	CMT	CMT				
Antarctic–Pacific	AnPc	An-Pc	CMT	CMT				
Bouvier	Bouv	An-Sa	CMT	CMT, EVC				
Antarctic-Scotia East	AnSc	An-Sc	CMT	EVC				
Burma	Burm	Au-Eu					CMT, EVC	
Java	Java	Au-Eu			CMT, EVC	CMT		CMT, EVC
Macquarie	MacQ	Au-Pc		CMT, EVC				
New Guinea	NGui	Au-Pc			CMT, EVC	CMT	CMT, EVC	
New Hebrides	Nheb	Au-Pc			CMT, EVC	CMT	CMT, EVC	
New Ireland	Nire	Au-Pc			CMT, EVC	CMT		CMT, EVC
New Zealand-N	NzeN	Au-Pc			CMT, EVC		CMT, EVC	
New Zealand-S	NzeS	Au-Pc			CMT, EVC		CMT, EVC	
Solomons	Solo	Au-Pc			CMT, EVC	CMT		CMT, EVC
Tonga-Kermadec	Toke	Au-Pc			CMT, EVC	CMT		CMT, EVC
Central America-S	CamS	Ca-Co			CMT, EVC	CMT	CMT, EVC	
Lesser Antilles	LAnt	Ca-Na			CMT, EVC		CMT, EVC	
Mexico	CAmN	Co-Na			CMT, EVC		CMT, EVC	
Cocos-Nazca	CoNz	Co-Nz	CMT	CMT				
Cocos–Pacific	CoPc	Co-Pc		CMT				
India	Indi	Eu-In			CMT, EVC	CMT		
Europe–North America	EuNa	Eu-Na	CMT	CMT, EVC				
Kurile-Hokkaido	KuHo	Eu-Pc			CMT, EVC	CMT		CMT, EVC
Philippines-N	PhiN	Eu-Ph			CMT, EVC	CMT		
Philippines-S	PhiS	Eu-Ph			CMT, EVC	CMT		CMT, EVC
Ryukyu-Taiwan	RyTa	Eu-Ph					CMT, EVC	
Juan de Fuca Ridge	JFri	Jf-Pc	CMT	CMT, EVC				
Aleutians	Aleu	Na-Pc			CMT, EVC	CMT	CMT, EVC	
California	Calf	Na-Pc	CMT	CMT, EVC				
Nazca-Pacific	NzPc	Nz-Pc	CMT	CMT				
South America	SoAm	Nz-Sa			CMT, EVC	CMT		CMT, EVC
Izu-Bonin-Marianas	IzBM	Pc-Ph			CMT, EVC	CMT		CMT, EVC
Scotia	ScoS	Sa-Sc			CMT, EVC		CMT, EVC	

and 3). The Nazca–Pacific boundary had the fastest velocity at 14 cm yr^{-1}, almost twice as great as the Antarctic–Pacific and Antarctic–Australia boundaries; and the moment rates for all three boundaries were not significantly different. Thus there is no evidence that moment rates decrease for velocities exceeding 7.5 cm yr^{-1}. No normal-faulting earthquakes whatsoever occurred along a 17th boundary, the Cocos–Pacific boundary, with a velocity of about 10 cm yr^{-1}.

There is about a factor of six variation in moment rate values superimposed on the decreasing trend with velocity. This variation is evident both in differences among estimates for a single plate boundary as calculated using different methods (e.g. eq. 2 versus eq. 6) and also in differences among the 'preferred' rates (darker symbols in Fig. 3) for different boundaries having similar velocities (e.g. Cocos–Nazca and Antarctic–Nazca boundaries). However, the moment rates aren't obviously affected by whether the diverging plates are oceanic or continental, or whether normal-faulting earthquakes occur in isolated clusters along the plate boundary or nearly continuously along its entire length. For example, the relative plate velocity is about 1.5 cm yr^{-1} for both the Africa–Antarctica (AfAn) and Arabia–Eurasia (Red Sea) boundaries; both have nearly identical moment rates even though normal faulting earthquakes occur nearly continuously along the AfAn boundary involving oceanic plates, and occur in isolated clusters along the Red Sea boundary between continental plates.

The coupled thicknesses W_{div} along divergent boundaries are all between 40 m and 2 km (Fig. 3); for boundaries with velocities exceeding 4 cm yr^{-1} all are less than 400 m. This suggests that the majority of the plate motion is accommodated aseismically; that is, if the width W_{estimate} of the seismically active region is 10 km, the coupling coefficients C_{div} are between 0.004 and 0.20.

© 2007 The Authors, *GJI*, **171,** 909–920
Journal compilation © 2007 RAS

Table 3. Normalized moment rates r_{div} (eq. 8) along divergent boundaries as calculated by different methods for the GCMT catalogue (columns '1' to '4'). Column '1' is simple rate determined using eq. (2); in column '2' this rate is adjusted to a standard period of 100 yr using eq. (5). In column '3' the base rate is determined from number of events exceeding a threshold magnitude M_T of 5.5 before making time adjustment; in column '4' the base rate is determined from 10th largest earthquake if this exceeds the threshold. Asterisks (*) indicate preferred magnitude plotted as filled symbols in Fig. 3.

			GCMT catalogue						
	V (cm yr^{-1})	$L_\perp$ (km)	N	$N_{>5.5}$	N_{large}	r_{div} (10^{13} kg s^{-2})			
These adjusted rates calculated assuming $M_C = 6.75$; $\beta = 0.75$						1	2	3	4
AfAn	1.41	4710	137	42	28	1.31*	1.98	5.30	2.13
AfAu	2.86	4275	96	22	28	0.44	0.67	1.22	0.88*
AnAu	6.79	7614	37	12	28	0.11	0.16	0.13	0.12*
AnNz	5.72	1535	37	13	28	0.26	0.39	0.84	0.64*
AnPc	7.58	5658	22	9	28	0.18	0.28	0.11*	–
AnSE	1.12	411	9	5	28	2.58	3.90	4.50*	–
AzGb	0.43	1555	13	5	28	1.50	2.27	3.11*	–
Bouv	1.66	642	15	7	28	2.09	3.15	3.04*	–
Calf	4.69	1015	17	6	28	0.40	0.60	0.55*	–
CoNz	5.34	2276	15	6	28	0.07	0.11	0.22*	–
EuNa	1.38	9147	195	45	28	0.88*	1.33	3.07	0.88
JFri	5.62	1362	20	5	28	0.14	0.21	0.27*	-
MAtR	2.31	3250	90	34	28	1.01*	1.53	3.56	2.58
NzPc	13.97	6017	30	18	28	0.04	0.06	0.14	0.12*
RedS	1.67	2762	47	13	28	0.62	0.94	1.61	1.25*
SAtR	3.20	8837	201	64	28	0.47*	0.72	2.19	0.60

3.2 Transform plate boundaries

Along 18 transform boundaries the moment rates generally decrease about a factor of 20 as the relative velocity increases from less than 1 cm yr^{-1} to about 14 cm yr^{-1}r (Fig. 4 and Tables 2 and 4). Since our moment rate calculation involves division by the relative velocity V, if we don't perform this normalization our result is equivalent to the statement that seismic moment per unit length of plate boundary is nearly independent of V. However, for transform boundaries, moment rates as we normalize them are about a factor of 10 and more higher than for divergent boundaries, although for boundaries with velocities less than about 2 cm yr^{-1} there is some overlap.

A factor of six variation in moment rates includes the majority of the measurements; however, rates along several boundaries fall well outside this range. For a few individual boundaries the different methods for calculating rates lead to a considerable range of estimates; for example, two orders of magnitude for the Australia–Pacific boundary south of New Zealand (along the Macquarie Ridge – labelled 'MacQ' in Fig. 4). The highest value was determined from the simple sum of GCMT moments (eq. 2) which included two earthquakes with $M_W \sim 8.1$ which occurred on 1989 May 23 and 2004 December 23. Another notable outlier was the Juan de Fuca–Pacific boundary ('JFri' in Fig. 4); since 1900 this relatively short boundary has experienced six earthquakes with magnitudes of 7 or greater (largest: 2005 June 15 with $M_W = 7.3$). A third outlier is the Europe–North America boundary ('EuNa' in Fig. 4) where the moment rates are a factor of 2010 less than along other boundaries with similar velocities. For EuNa the largest observed earthquakes seem to have magnitudes of 7 or less; this contrasts with the Africa–Antarctic boundary, where one of the largest known oceanic strike-slip earthquakes occurred on 1942 November 10 (see Okal & Stein 1987).

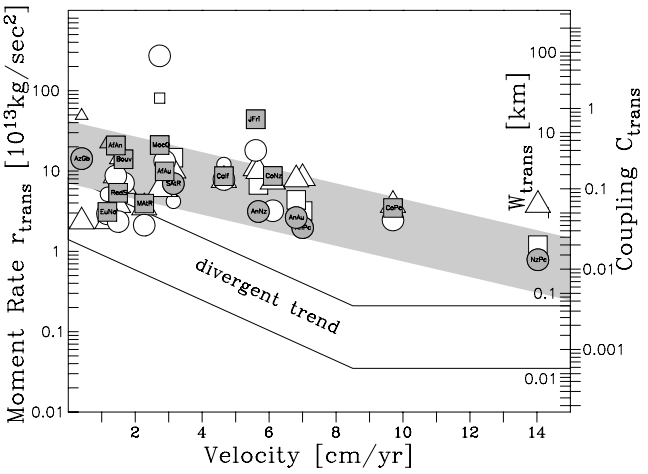


Figure 4. Transform plate boundaries: Dependence on relative plate velocity of moment rate r_{trans} (eq. 8), coupled thickness W_{trans} (see eq. 9) and coupling coefficient C_{trans} (see eq. 10) Larger symbols are strike-slip GCMT events occurring 1977–2005 along transform plate boundaries; smaller symbols are events in the combined GCMT-EVC catalogue. Symbols are as in Fig. 3. All calculations assume $\beta = 0.75$, $\mu = 30$ GPa and a cut-off moment M_C as indicated in Table 4; calculation of W_{trans} assumes $W_{estimate} = 20$ km. Shaded region indicates approximate trend of the data.

Except for the Juan de Fuca–Pacific and Nazca–Pacific boundaries, the coupled thicknesses W_{trans} are all between 800 m and 8 km (Fig. 4). This suggests that the majority of the plate motion is accommodated aseismically; that is, if the width $W_{estimate}$ of the seismically active region is 20 km, the coupling coefficients C_{trans} are between 0.04 and 0.40.

3.3 Convergent plate boundaries (shallow thrusts)

Along 20 convergent boundaries (Fig. 5 and Tables 2 and 5) there is no obvious dependence on plate convergence velocity and nearly all rates are at least 2–10 times higher than typical rates along transform boundaries. The majority have convergence velocities between 7 and 11 cm yr^{-1} and have moment rates in the range of 20–200 $\times$ 10^{13} kg s^{-2}. These included the four convergent boundaries that have experienced earthquakes with magnitudes of 9.0 or greater (Aleutians, South America, Kurile-Hokkaido and Java). In this group weakly coupled boundaries between two oceanic plates (Izu-Bonin-Marianas, Tonga-Kermadec and Scotia) all had preferred moment rates at the low end of the range, that is, about 20 $\times$ 10^{13} kg s^{-2}.

© 2007 The Authors, *GJI*, **171,** 909–920
Journal compilation © 2007 RAS

Table 4. Normalized moment rates r_{trans} (eq. 8) along transform boundaries as calculated by different methods for strike-slip earthquakes in the GCMT catalogue (columns '1' to '4') and all events in the combined EVC-GCMT catalogues (columns labelled '5' to '8'). Columns '1' and '5' are simple rates determined using eq. (2); in columns '2' and '6' this rate is adjusted to a standard period of 100 yr using eq. (5). In columns '3' and '7' the base rate is determined from number of events exceeding a threshold magnitude (5.5 for GCMT and 6.84 for EVC) before making time adjustment; in columns '4' and '8' the base rate is determined from 10th largest earthquake if this exceeds the threshold. Asterisks (*) indicate preferred magnitude plotted as filled symbols in Fig. 4.

	GCMT catalogue.									combined EVC-GCMT catalogue						
	V (cm yr^{-1})	$L_{\|\|}$ (km)	N	$N_{>5.5}$	N_{large}	r_{trans} (10^{13} kg s^{-2})				N	$N_{>6.84}$	N_{large}	r_{trans} (10^{13} kg s^{-2})			
						1	2	3	4				5	6	7	8
These adjusted rates calculated assuming $M_C = 7.2$; $\beta = 0.75$																
AnAu	6.81	4995	283	191	91	2.64*	3.98	7.83	4.37	444	0	3	–	–	–	–
AnNz	5.68	2763	169	128	91	3.14*	4.74	9.95	6.71	243	0	3	–	–	–	–
AnPc	7.00	3979	251	169	91	1.97*	2.98	8.12	3.18	352	2	3	–	–	–	–
CoNz	6.11	1183	93	57	91	3.20	4.84	7.34*	8.67	153	2	3	–	–	–	–
CoPc	9.70	408	30	22	91	2.46	3.71	3.77*	3.47	45	2	3	–	–	–	–
EuNa	1.17	5760	59	23	91	2.93	4.43	2.36*	3.09	366	4	3	5.12	5.03	4.78	–
JFri	5.60	1047	112	65	91	18.05	27.27	10.79*	44.07	171	7	3	8.69	8.52	11.54	–
MAtR	2.27	1763	37	21	91	2.12	3.20	3.50*	3.94	164	1	3	–	–	–	–
NzPc	14.03	2652	172	118	91	0.79*	1.19	3.76	1.19	276	1	3	–	–	–	–
RedS	1.49	2343	32	20	91	2.35	3.55	3.76*	5.36	104	1	3	–	–	–	–
SAtR	3.14	7142	262	169	91	6.97*	10.54	10.08	14.67	569	15	3	4.19	4.11	8.33	8.43
These adjusted rates calculated assuming $M_C = 7.6$; $\beta = 0.75$																
AfAu	2.88	3102	96	57	256	13.26	20.03	5.94*	9.91	248	2	7	–	–	–	–
AnSE	1.13	1314	5	2	256	–	–	–	–	33	4	7	27.93	27.40	21.59*	–
Bouv	1.65	1562	30	24	256	7.09	10.72	6.50*	13.99	66	5	7	16.56	16.24	16.75	–
Calf	4.65	3013	151	97	256	7.84	11.85	7.70*	8.62	282	22	7	12.06	11.83	22.21	19.05
These adjusted rates calculated assuming $M_C = 8.1$; $\beta = 0.75$																
AfAn	1.42	4871	94	63	933	8.67	13.09	8.79	20.80*	305	9	26	22.12	21.69	13.69	–
AzGb	0.40	2192	11	5	933	14.26*	21.54	2.34	–	45	5	26	293.40	287.76	48.90	–
MacQ	2.73	1651	52	34	933	271.37	409.97	5.92	21.06*	13	18	26	148.75	145.89	52.88	80.89

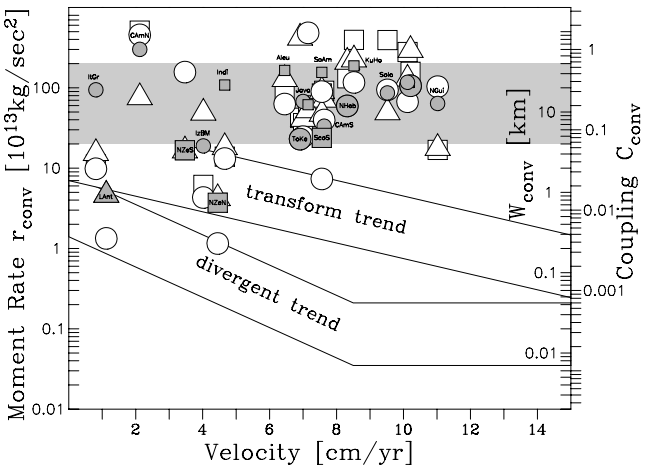


Figure 5. Convergent plate boundaries – thrust earthquakes: Dependence on relative plate velocity of moment rate r_{conv} (eq. 8), coupled thickness W_{conv} (see eq. 9) and coupling coefficient C_{conv} (see eq. 10). Larger symbols are thrust GCMT events occurring 1977–2005 along convergent plate boundaries; smaller symbols are events in the combined GCMT-EVC catalogue. Symbols are as in Fig. 3. All calculations assume $\beta = 0.60$, $\mu = 50$ GPa, and a cutoff moment M_C as indicated in Table 5; calculation of W_{conv} assumes $W_{estimate} = 60$ km. Shaded region indicates approximate trend of the data.

The moment rates that are anomalously high and low all are from boundaries with velocities of 6 cm yr^{-1} or less. Of these, the rates for the Lesser Antilles and North Island, New Zealand, are anomalously low; both of these regions possessed relatively few earthquakes and it is possible this affects the measurements. In contrast, Mexico ('CAmN' in Fig. 5) had the highest moment rate; this came about because it has experienced no fewer than 10 earthquakes with magnitudes of 7.6 or greater, including three since 1977.

The coupled thicknesses W_{conv} along convergent boundaries were mostly between 4 and 40 km (Fig. 5). If the width $W_{estimate}$ of the seismically active region is 60 km, the coupling coefficients C_{conv} are between 0.07 and 0.7. If we compute values for all convergent boundaries taken together (mean of the preferred values in Table 5 weighted by plate boundary length L), we obtain W_{conv} of 20 km and C_{conv} of 0.33. We note that C_{conv} is 0.1 or less for the weakly coupled boundaries between two oceanic plates (Tonga-Kermadec, Izu-Bonin-Marianas and Scotia) whereas it is on the order of 0.6–1.0 for the strongly coupled boundaries where the overriding plate is continental (Aleutians, Kurile-Hokkaido, Mexico and South America).

3.4 Convergent plate boundaries (shallow strike-slip events)

Relative plate motion along so-called convergent plate boundaries is usually somewhat oblique and strike-slip earthquakes occur along many boundaries, although not as commonly as thrust earthquakes. Thus for completeness we determine moment rates for strike-slip earthquakes in the GCMT catalogue normalized by the parallel component $L_{||}$ of plate boundary length (Fig. 6 and Tables 2 and 6).

There is considerable variation in the moment rates for these events. However, strike-slip moment rates along most boundaries are somewhat less than for thrust earthquakes, but in approximately the same range as moment rates along transform boundaries. An exception is Central America, where the rates for thrust and strike-slip earthquakes are approximately the same.

© 2007 The Authors, *GJI*, **171,** 909–920
Journal compilation © 2007 RAS

Table 5. Normalized moment rates r_{conv} (eq. 8) along convergent boundaries as calculated by different methods for thrust earthquakes in the GCMT catalogue (columns '1' to '4') and all events in the combined EVC-GCMT catalogues (columns labeled '5' to '8'). Columns '1' and '5' are simple rates determined using eq. (2); in columns '2' and '6' this rate is adjusted to a standard period of 100 yr using eq. (5). In columns '3' and '7' the base rate is determined from number of events exceeding a threshold magnitude (5.5 for GCMT and 6.84 for EVC) before making time adjustment; in columns '4' and '8' the base rate is determined from 10th largest earthquake if this exceeds the threshold. Asterisks (*) indicate preferred magnitude plotted as filled symbols in Fig. 5.

	GCMT catalogue									combined EVC-GCMT catalogue							
	V (cm yr^{-1})	$L_\perp$ (km)	N	$N_{>5.5}$	N_{large}	r_{conv} (10^{13} kg s^{-2})				N	$N_{>6.84}$	N_{large}	r_{conv} (10^{13} kg s^{-2})			
						1	2	3	4				5	6	7	8
These adjusted rates calculated assuming $M_C = 8.2$; $\beta = 0.60$																
CAmN	2.12	1386	122	71	292	456.43	1041.77	75.93	514.80	226	46	17	300.82*	289.35	498.95	541.33
CAmS	7.63	1632	234	162	292	39.77	90.78	70.68	91.93	442	42	17	33.27*	32.00	100.93	45.21
ItGr	0.81	3358	58	26	292	9.83	22.43	15.32	11.18	392	27	17	94.35*	90.75	221.00	146.37
IzBM	4.02	2615	243	117	292	4.31	9.83	48.70	6.20	592	17	17	18.90*	18.18	26.49	19.01
LAnt	1.12	1128	23	8	292	1.34	3.05	4.63*	–	62	2	17	10.46	10.07	6.22	–
NGui	11.02	861	131	60	292	103.36	235.92	17.72	16.85	355	27	17	63.77*	61.34	63.43	42.01
NHeb	8.32	1481	531	309	292	59.49*	135.79	209.60	131.26	1096	80	17	67.43	64.86	298.61	91.19
NIre	10.21	903	521	318	292	106.07*	242.10	293.89	158.18	1206	78	17	124.62	119.87	382.64	172.17
NZeN	4.45	702	26	13	292	1.15	2.63	4.21	3.71*	129	5	17	22.73	21.86	11.59	–
NZeS	3.47	174	14	11	292	156.83	357.95	16.49	16.72*	24	6	17	53.77	51.72	81.36	–
PhiN	7.00	1896	217	121	292	24.67	56.31	40.78	36.38	707	69	17	67.64*	65.07	216.64	119.58
PhiS	10.12	781	280	177	292	67.10	153.16	129.13	279.30	578	58	17	117.13*	112.67	272.44	100.67
ScoS	7.56	650	184	108	292	7.34	16.74	91.02	23.81*	302	10	17	30.79	29.62	23.37	28.75
Solo	9.52	463	126	70	292	94.35	215.35	49.30	393.00	321	41	17	86.32*	83.03	273.85	100.28
ToKe	6.91	2330	1029	549	292	22.98*	52.45	418.16	42.37	1679	59	17	79.66	76.62	137.60	139.27
These adjusted rates calculated assuming $M_C = 9.5$; $\beta = 0.60$																
Aleu	6.45	2788	529	288	4325	62.83	143.40	127.80	83.99	1078	81	248	489.24	470.60	209.02	164.45*
Indi	4.66	3142	217	79	4325	13.16	30.03	18.16	13.90	610	51	248	68.42	65.81	118.63	108.38*
Java	7.15	5094	639	257	4325	483.73	1104.10	52.16	60.60	1671	71	248	166.97	160.61	82.81	61.56*
KuHo	8.52	2896	970	488	4325	116.56	266.05	224.06	394.76	1679	157	248	308.52	296.76	458.48	187.56*
SoAm	7.56	5746	431	269	292	89.62	204.56	47.19	85.30	861	105	305	641.49	617.05	133.27	155.87*

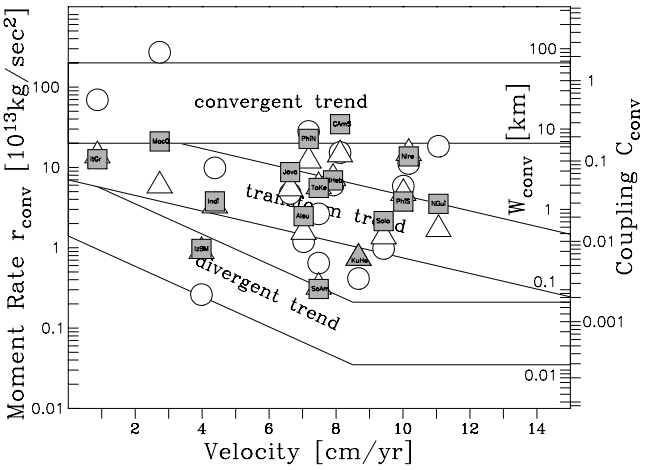


Figure 6. Convergent plate boundaries – strike-slip earthquakes: Dependence on relative plate velocity of moment rate r_{conv} (eq. 8), coupled thickness W_{conv} (see eq. 9) and coupling coefficient C_{conv} (see eq. 10). Symbols indicate moment rates for strike-slip GCMT earthquakes occurring 1977–2005 along convergent plate boundaries. Symbols are as in Fig. 3. All calculations assume $\beta = 0.75$, $\mu = 30$ GPa and a cutoff moment M_C of 7.6 (see Table 6); calculation of W_{conv} assumes $W_{estimate} = 40$ km.

3.5 Intermediate and deep-focus earthquakes

For boundaries with intermediate-depth earthquakes (Fig. 7 and Table 7), moment rates decrease steadily with depth from values of about 100 × 10^{13} kg s^{-2} at shallow depths, and are in the range of 1–5 × 10^{13} kg s^{-2} at depths of 100–200 km. This corresponds to coupling C_{int} of 0.01–0.05. Between 200 and 300 km depth, moment rates and C_{int} fall off even further and are less than 0.1 × 10^{13} kg s^{-2} and 0.001, respectively, at 280–300 km.

Moment rates for boundaries with deep-focus earthquakes (Fig. 8 and Table 8) are virtually identical to the intermediate-depth rates from the surface down to 300 km depth where they reach a minimum. However, between 320 and about 540 km the rates are again in the 1–5×10^{13} kg s^{-2} range, and at still greater depths they are a factor of 2–4 higher still, at 620–640 km rates are possibly are even greater than at 100–200 km. Rates drop off beneath 640 km; the relatively higher rate at 680–700 km may not be higher as it is due to a single earthquake with M_W of 7.7 which occurred on 2002 August 19 and which the GCMT catalogue assigns a depth of 699 km.

4 DISCUSSION

How important are earthquakes to plate tectonics; that is, how much of the relative motion between plates is expressed by seismic slip? The 30–100 yr of data that is presently available clearly demonstrates that along transform, divergent, intermediate and deep boundaries the answer is 'slip is mostly aseismic'; along nearly all of these boundaries, estimates of the coupling coefficient C were less than 0.4. For shallow earthquakes along convergent boundaries the answer is more complicated; slip is mostly aseismic ($C_{conv} < 0.1$) when the converging plates are both oceanic as in Tonga-Kermadec, the Marianas-Izu-Bonin and the Scotia arcs. However, nearly all or at least the majority of the slip is seismic ($C_{conv} \sim 0.6$–1.0) when the overriding plate is continental, as in Alaska, Mexico and South America.

Thus, like Bird & Kagan (2004) and other previous studies, the present investigation finds that rates of moment release are significantly different along divergent, transform, convergent and deep

Table 6. Normalized moment rates r_{conv} (eq. 8) for strike-slip earthquakes in the GCMT catalogue along convergent boundaries as calculated by different methods (columns '1' to '4'). Column '1' is simple rate determined using eq. (2); in column '2' this rate is adjusted to a standard period of 100 yr using eq. (5). In column '3' the base rate is determined from number of events exceeding a threshold magnitude M_T 0f 5.5 before making time adjustment; in column '4' the base rate is determined from 10th largest earthquake if this exceeds the threshold. Asterisks (*) indicate preferred magnitude plotted as filled symbols in Fig. 6.

	GCMT catalogue								
	V (cm yr^{-1})	$L_\perp$ (km)	N	$N_{>5.5}$	N_{large}	r_{conv} (10^{13} kg s^{-2})			
						1	2	3	4
These adjusted rates calculated assuming $M_C = 7.6$; $\beta = 0.75$									
Aleu	7.03	1868	51	28	256	1.19	1.80	1.57	2.48*
CAmS	8.12	112	31	20	256	15.31	23.13	14.44	34.52*
Indi	4.38	2343	91	41	256	9.86	14.90	3.34	3.77*
ItGr	0.87	2093	63	33	256	69.43	104.90	14.05	12.63*
IzBM	3.98	1850	27	12	256	0.26	0.39	0.90	0.97*
Java	6.63	4011	288	121	256	4.74	7.17	5.44	8.75*
KuHo	8.67	703	19	9	256	0.41	0.63	0.74*	–
NGui	11.06	992	45	26	256	18.34	27.71	1.70	3.52*
NHeb	7.91	686	82	46	256	6.03	9.11	7.35	6.88*
NIre	10.17	1227	223	147	256	11.20	16.92	15.05	13.68*
PhiN	7.18	474	95	47	256	28.03	42.35	12.07	22.69*
PhiS	10.01	834	62	46	256	5.85	8.83	4.78	3.76*
SoAm	7.48	2433	25	11	256	0.64	0.97	0.33	0.31*
Solo	9.42	752	29	16	256	0.98	1.48	1.38	2.15*
ToKe	7.48	868	65	44	256	2.64	3.99	5.79	5.56*

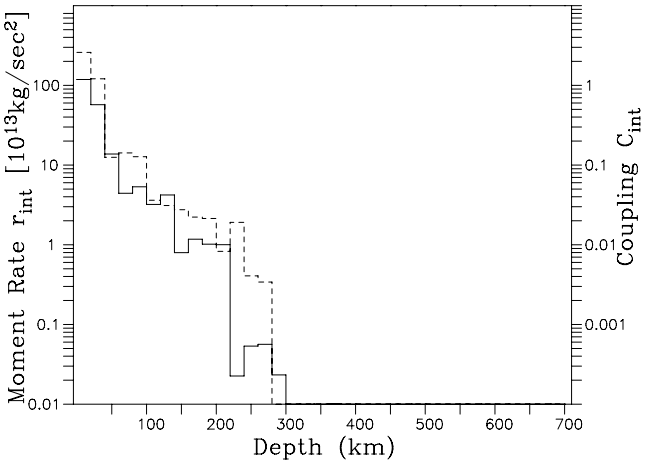


Figure 7. Convergent plate boundaries with intermediate-depth earthquakes: Dependence on depth of moment rate r_{int} (see Section 2.3) and coupling coefficient C_{int} (eq. 11). Solid line indicates moment rates for GCMT earthquakes occurring 1977–2005 along plate boundaries where the deepest earthquakes are 300 km and less; dashed lines are results from the EVC catalogue. Conversion for right-hand scale for C_{int} assumes θ is 45° and μ is 70 GPa; results for C_{int} assuming μ varies with depth are in Table 7. Plotted rates are determined from simple rate (eq. 2) and have not been time-adjusted. Geographic regions included are: Aleutians, Burma, Caribbean, Central America, Greece, Mexico, New Guinea, New Hebrides, New Zealand, Ryukyu, Scotia and Taiwan.

plate boundaries. Although there is about an order of magnitude variation among the rates within each group, the variation between groups is even larger and thus implies that there are profound differences in the mechanical processes along the different kinds of boundaries. It is generally recognized that the physical mechanisms responsible for deep and shallow earthquakes must be fundamentally different (e.g. Green & Houston 1995; Frohlich 2006); however, shallow-focus earthquakes along divergent, transform and convergent margins are all thought to be brittle fracture. The large variation in moment rates between the three shallow groups suggests that they are also fundamentally different mechanically but what exactly is responsible for this mechanical difference (temperature, mineral composition and differential hydration) is beyond the scope of this paper (for a discussion, see Boettcher & Jordan 2004).

These results have implications for earthquake prediction research. First, because plate tectonic motion is largely aseismic along most plate boundaries, the analysis of seismicity patterns alone may fail to yield a reliable predictor of large earthquakes. Properly interpreting the significance of seismic gaps or changes in the rate of seismicity would seem to require knowledge of aseismic plate motion, such as might be measured by continuously recording GPS networks. And second, it seems likely that different kinds of plate boundaries will require completely different prediction algorithms. If we found an algorithm that successfully forecasts earthquakes in Alaska or South America, both convergent boundaries where earthquakes reflect a majority of the relative plate motion, there is no reason to expect that any similar algorithm would work in California, a strike-slip boundary where the coupling C_{trans} is about 0.20.

Within each category of plate boundary the observed moment rates show variations of about an order of magnitude, even after accounting for differences related to relative plate velocity (Figs 3–6). Some of this is simply the measurement uncertainty discussed in Frohlich (2007) and Section 2.1 above, that is, the influence on calculated rates of large earthquakes and/or assumptions made about the value of β. For individual boundaries the uncertainties are clearly evident in the rate values calculated using different methods (Tables 3–6); the different methods often find rates that differ by an order of magnitude or more. Along the Macquarie Ridge Complex, for example, two M_W 8.1 earthquakes in 1989 and 2004 cause the simple moment rate (eq. 2) to be 271×10^{13} kg s^{-2}, as compared to 21×10^{13} kg s^{-2} as determined from the tenth largest GCMT earthquake. Also, the present study has taken a whole-plate-boundary approach to evaluating moment rates; thus, to calculate rates we

© 2007 The Authors, *GJI*, **171,** 909–920
Journal compilation © 2007 RAS

Table 7. Normalized moment rates r_{int} (eq. 8) and coupling coefficients C_{int} for earthquakes in the GCMT and EVC catalogues along nine convergent boundaries where deepest earthquakes are ∼300 km or less. Rates in table (see also Fig. 7) are determined from simple rates (eq. 2) and are not adjusted to a standard time period. Coupling coefficients C_{int} are calculated from eq. (11) assuming $\theta = 45^\circ$ and values for rigidity μ at each depth as reported by Stacey (1992); thus coupling coefficients differ from those in Fig. 7.

Depth (km)	GCMT catalogue			EVC catalogue		
	N_{CMT} (10^{13} kg s^{-2})	r_{int}	C_{int}	N_{EVC} (10^{13} kg s^{-2})	r_{int}	C_{int}
0–20	2411	118.5200	0.5740	2947	259.4000	0.8559
20–40	1239	57.1490	0.0896	1702	120.8700	0.2429
40–60	429	13.7610	0.0262	607	12.5310	0.0326
60–80	175	4.4225	0.0060	248	14.2210	0.1106
80–100	151	5.3356	0.0080	216	12.7330	0.0362
100–120	167	3.2080	0.0057	207	3.6154	0.0064
120–140	104	4.2188	0.0139	139	3.1058	0.0077
140–160	69	0.7959	0.0012	101	2.7573	0.0060
160–180	49	1.1757	0.0016	68	2.2242	0.0033
180–200	44	1.0161	0.0014	54	2.1358	0.0030
200–220	30	1.0024	0.0015	37	0.8281	0.0012
220–240	14	0.0226	0.0001	25	1.9121	0.0024
240–260	14	0.0536	0.0001	16	0.4076	0.0005
260–280	11	0.0563	0.0003	15	0.3407	0.0008
280–300	2	0.0233	0.0000	2	0.0062	0.0000

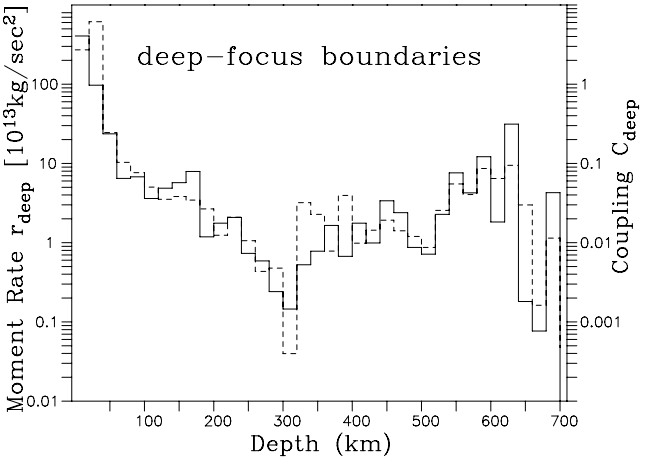


Figure 8. Convergent plate boundaries with deep-focus earthquakes: Dependence on depth of moment rate r_{deep} (see Section 2.3) and coupling coefficient C_{deep} (eq. 11). Solid line indicates moment rates for GCMT earthquakes occurring 1977–2005 along plate boundaries where the deepest earthquakes are 500–700 km; dashed lines are results from the EVC catalogue. Conversion for right-hand scale for C_{deep} assumes θ is 45° and μ is 70 GPa; results for C_{deep} assuming μ varies with depth are in Table 8. Plotted rates are determined from simple rate (eq. 2) and have not been time-adjusted. Geographic regions included are: Italy, Izu-Bonin, Japan-Kuriles, Java, Marianas, New Ireland, Philippines, South America, Solomons and Tonga-Kermadec.

divide by the length $L_{||}$ or $L_{\perp}$ determined for the entire plate boundary, even when no earthquakes have occurred along long segments of the boundary. In these cases it isn't clear whether these segments are truly aseismic, or whether seismic activity is episodic such that over observation periods spanning centuries or millennia activity would fill in the currently inactive segments. However, it is perhaps surprising that there isn't more rate variation considering the variations in tectonic environment within individual groups. For transform boundaries, the preferred moment rates for the Africa–Antarctica and Macquarie boundaries are nearly identical, as are the rates for California and the Cocos–Nazca boundaries.

The results of this study are in general agreement with Bird & Kagan (2004), but there were some differences. Both studies obtained comparable results for coupled thickness W and seismic coupling C for oceanic normal faulting earthquakes and for thrust earthquakes along ocean–ocean and ocean–continent boundaries. For strike-slip events along oceanic transforms our study found lower values for W and C for slow (V < 4 cm yr^{-1}) and fast ($V >$ 7 cm yr^{-1}) transforms, but similar values at intermediate velocities. Bird and Kagan considered continent–continent boundaries as separate categories; the present study lumped them together but found results for them that were within the range of values obtained for other categories. The present study evaluated moment release for slip along intermediate and deep-focus boundaries and finds that for depths of 100–650 km the seismic coupling is relatively low—generally about 0.01–0.05—values comparable to normal-faulting earthquakes along oceanic ridge-transforms and more than an order of magnitude lower than many strike-slip or thrust boundaries.

ACKNOWLEDGMENTS

This research came about because of support from the Incorporated Research Institutions for Seismology through a Sabbaticals in Seismology grant to Laura Wetzel. This work could not have been completed without invaluable babysitting support from Jackie Henkel and Jim Wetzel.

REFERENCES

Abe, K., 1981. Magnitudes of large shallow earthquakes from 1904 to 1980, *Phys. Earth Planet. Int.,* **27,** 72–92.

Abe, K., 1984. Complements to magnitudes of large shallow earthquakes from 1904 to 1980, *Phys. Earth Planet. Int.,* **34,** 17–23.

Båth, M. & Duda, S.J., 1979. *Some Aspects of Global Seismicity,* Rept. 1–79, Seismological Institute, Uppsala, Sweden.

Bird, P. & Kagan, Y.Y., 2004. Plate-tectonic analysis of shallow seismicity: apparent boundary width, beta, corner magnitude, coupled lithosphere thickness, and coupling in seven tectonic settings, *Bull. seism. Soc. Am.,* **94,** 2380–2399.

Table 8. Normalized moment rates r_{deep} (eq. 8) and coupling coefficients C_{deep} for earthquakes in the GCMT and EVC catalogues along convergent boundaries where deepest earthquakes extend to depths of 500–700 km (see Table 2). Rates in table (see also Fig. 8) are determined from simple rates (eq. 2) and are not adjusted to a standard time period. Coupling coefficients C_{deep} are calculated from eq. (11) assuming $\theta = 45^\circ$ and values for rigidity μ at each depth as reported by Stacey (1992); thus coupling coefficients differ from those in Fig. 8.

Depth (km)	GCMT catalogue			EVC catalogue		
	N_{CMT} (10^{13} kg s^{-2})	r_{deep}	C_{deep}	N_{EVC} (10^{13} kg s^{-2})	r_{deep}	C_{deep}
0–20	4895	405.8700	1.1460	5792	271.2100	0.7581
20–40	2806	97.2680	0.1827	3746	614.7200	0.9908
40–60	1242	23.6420	0.0419	1662	24.5640	0.0471
60-80	505	6.4796	0.0090	650	10.3330	0.0698
80–100	478	6.7877	0.0137	620	7.6535	0.0246
100–120	440	3.6089	0.0067	565	5.0231	0.0096
120–140	385	4.8629	0.0122	453	3.5252	0.0086
140–160	253	5.7267	0.0145	313	3.8197	0.0083
160–180	160	7.9252	0.0113	215	3.4459	0.0057
180–200	123	1.1838	0.0017	159	2.6720	0.0055
200–220	100	1.7615	0.0028	126	1.2401	0.0023
220–240	75	2.0814	0.0069	85	2.0970	0.0037
240–260	55	0.7327	0.0011	70	1.0606	0.0014
260–280	61	0.5882	0.0010	72	0.4336	0.0006
280–300	35	0.2410	0.0004	42	0.4775	0.0007
300–320	29	0.1455	0.0002	31	0.0399	0.0001
320–340	27	0.5263	0.0006	41	3.1974	0.0070
340–360	42	0.7806	0.0011	63	2.2750	0.0032
360–380	49	1.6487	0.0025	58	0.7821	0.0010
380–400	52	0.6730	0.0011	64	3.9525	0.0047
400–420	42	1.7637	0.0034	57	0.9856	0.0016
420–440	37	0.9907	0.0017	47	1.4368	0.0017
440–460	36	3.3784	0.0048	46	1.9198	0.0025
460–480	32	2.3939	0.0022	42	1.4113	0.0017
480–500	71	0.8698	0.0011	82	1.1975	0.0019
500–520	68	0.7152	0.0008	79	0.8711	0.0009
520–540	110	2.2783	0.0024	132	2.5577	0.0023
540–560	115	7.6014	0.0065	150	5.5104	0.0049
560–580	163	4.2580	0.0043	198	4.0486	0.0037
580–600	185	12.1470	0.0113	228	8.6394	0.0077
600–620	127	1.8246	0.0015	154	6.4533	0.0054
620–640	69	31.3600	0.0277	90	9.4668	0.0084
640–660	23	0.1807	0.0001	38	2.9928	0.0025
660–680	12	0.0767	0.0001	14	0.1623	0.0003
680–700	4	4.2814	0.0032	4	1.1417	0.0008

Bird, P., Kagan, Y. & Jackson, D.D., 2002. Plate tectonics and earthquake potential of spreading ridges and oceanic transform faults, in *Plate Boundary Zones, Geodynamic Series* Vol. **30**, pp. 203–218, eds Stein, S. & Freymueller, J.T., Amer. Geophys. Un., Washington, DC.

Boettcher M.S. & Jordan, T. H, 2004. Earthquake scaling relations for mid-ocean ridge transform faults, *J. geophys. Res.,* **109,** B12302. doi:10.1029/2004JB003110.

Brune, J.N.,1968. Seismic moment, seismicity, and rate of slip along major fault zones, *J. geophys. Res.,* **73,** 777–784.

Chen, P.-F., Nettles, M., Okal, E.A. & Ekström, G., 2001. Centroid moment tensor solutions for intermediate-depth earthquakes of the WWSSN-HLGP era (1962–1975), *Phys. Earth Planet. Int.,* **124,** 1–7. doi:10.1016/S0031–9201(00)00220-X.

Coffin, M.F., Gahagan, L.M. & Lawver, L., 1998. *Present-Day Plate Boundary Digital Data Compilation,* Univ. Texas Inst. Geophys. Tech. Rept. No. 174, 5 pp.

DeMets, C., Gordon, R.G., Argus, D.F. & Stein, S., 1994. Effect of recent revisions to the geomagnetic reversal timescale on estimates of current plate motions, *Geophys. Res. Lett.,* **21,** doi:10.1029/94GL02118, 2191–2194.

Dziewonski, A.M. & Woodhouse, J.H., 1983. Studies of the seismic source using normal-mode theory, in *Earthquakes: Observation, Theory and Interpretation,* pp. 45–137, eds H. Kanamori and E. Boschi, North-Holland, New York.

Ekström, G., Dziewonski, A.M., Maternovskaya, N.N. & Nettles, M., 2005. Global seismicity of 2003: centroid-moment-tensor solutions for 1087 earthquakes, *Phys. Earth Planet. Int.,* **148,** 327–35.

Engdahl, E.R. & Villaseñor, A., 2002. Global seismicity: 1900–1999, in *International Handbook of Earthquake and Engineering Seismology,* Int. Assoc. Seismol. Earth's Interior, San Diego, CA, pp. 665–690.

Frohlich, C., 2001. Display and and quantitative assessment of distributions of earthquake focal mechanisms, *Geophys. J. Int.,* **144,** 300–308.

Frohlich, C., 2006. *Deep Earthquakes,* Cambridge Univ. Press, Cambridge, UK, 574 pp.

Frohlich, C., 2007. Practical suggestions for assessing rates of seismic moment release, *Bull. seism. Soc. Am.,* **97,** doi:10.1785/0120060193, 1158–1166.

Frohlich, C. & Davis, S.D., 1993. Teleseismic b values; Or, much ado about 1.0, *J. geophys. Res.,* **98,** 631–644.

Frohlich, C. & Davis, S.D., 1999. How well constrained are well-constrained T, B, and P axes in moment tensor catalogs? *J. geophys. Res.,* **104,** doi:10.1029/1998JB900071, 4901–4910.

Green, H.W. & Houston, H., 1995. The mechanics of deep earthquakes, *Ann. Rev. Earth Planet. Sci.,* **23,** 169–213.

© 2007 The Authors, *GJI*, **171,** 909–920
Journal compilation © 2007 RAS

Gutenberg, B. & Richter, C.F., 1954. *Seismicity of the Earth and Associated Phenomena,* Princeton Univ. Press, Princeton, NJ, 310 pp.

Gutenberg, B. & Richter, C.F., 1956. Magnitude and energy of earthquakes, *Ann. Geof,* **9,** 1–15.

Huang, W.-C., Okal, E.A., Ekström, G. & Salganik, M.P., 1997. Centroid moment tensor solutions for deep earthquakes predating the digital era: the World-Wide Standardized Seismograph Network dataset (1962–1976), *Phys. Earth Planet. Int.,* **99,** doi:10.1016/S0031–9201(96)03177–9, 121–129.

Huang, W.-C., Okal, E.A., Ekström, G. & Salganik, M.P., 1998. Centroid moment tensor solutions for deep earthquakes predating the digital era: the historical dataset (1907–1961), *Phys. Earth Planet. Int.,* **106,** 181–190. doi:10.1016/S0031–9201(98)00081–8

Ishimoto, M. & Iida, K., 1939. Observations of earthquakes registered with microseismographs constructed recently (in Japanese), *Bull. Earthquake Res. Inst., Tokyo Univ.,* **17,** 443–478.

Jarrard, R.D., 1986. Relations among subduction parameters, *Rev. Geophys.,* **24,** 217–284.

Kagan, Y.Y., 1997. Seismic moment-frequency relation for shallow earthquakes: regional comparisons, *J. Geophys. Res.,* **102,** 2835–2852.

Kagan, Y.Y., 1999. Universality of the seismic moment-magnitude relation, *Pure Appl. Geophys.,* **155,** 537–573.

McCaffrey, R., 1997a. Influences of recurrence times and fault zone temperatures on the age-rate dependence of subduction zone seismicity, *J. geophys. Res.,* **102,** 22 839–22 854.

McCaffrey, R., 1997b. Statistical significance of the seismic coupling coefficient, *Bull. seism. Soc. Am.,* **87,** 1069–1073.

Okal, E.A. & Stein, S., 1987. The 1942 Southwest Indian Ocean Ridge earthquake: largest ever recorded on an oceanic transform, *Geophys. Res. Lett.,* **14,** 147–1950.

Pacheco, J.F. & Sykes, L.R., 1992. Seismic moment catalog of large shallow earthquakes, 1900 to 1989, *Bull. seism. Soc. Am.* **82,** 1306–1349.

Pacheco, J.F., Sykes, L.R. & and Scholz, C.H., 1993. Nature of seismic coupling along simple plate boundaries of the subduction type, *J. geophys. Res.,* **98,** 14 133–14 159.

Peterson, E.T. & Seno, T., 1984. Factors affecting seismic moment release rates in subduction zones, *J. geophys. Res.,* **89,** 10 233–10 248.

Rothé, J.P., 1969. *The Seismicity of the Earth, 1953–1965,* United Nations Educational, Scientific and Cultural Organization (UNESCO), Paris, 336 pp.

Rundquist, D.V. & Sobolev, P.O., 2002. Seismicity of mid-oceanic ridges and its geodynamic implications: a review, *Earth Sci. Rev.,* **58,** 143–161.

Scholz, C.H., 2002. *The Mechanics of Earthquakes and Faulting,* 2nd edn, Cambridge Univ. Press, Cambridge, UK, pp. 471.

Solomon, S.C., Huang, P.Y. & Meinke, L., 1988. The seismic moment budget of slowly spreading ridges, *Nature,* **334,** 58–60.

Stacey, F.D., 1992. *Physics of the Earth,* 3rd edn, Brookfield Press, Brisbane, Australia, 513 pp.

Tichelaar, B.W. & Ruff, L.J., 1993. Depth of seismic coupling along subduction zones, *J. geophys. Res.,* **98,** 2017–2037

Utsu, T., 2002. Relationship between magnitude scales, in *International Handbook of Earthquake and Engineering Seismology,* Int. Assoc. Seismol. Earth's Interior, San Diego, CA, pp. 733–746.